

Ultrafast dynamics of non-equilibrium electrons and strain generation under femtosecond laser irradiation of Nickel

George D.Tsibidis *

Institute of Electronic Structure and Laser (IESL), Foundation for Research and Technology (FORTH), N. Plastira 100, Vassilika Vouton, 70013, Heraklion, Crete, Greece

We present a theoretical study of the ultrafast electron dynamics in transition metals using ultrashort pulsed laser beams. The significant influence of the contribution of the dynamics of produced nonthermal electrons to electron thermalisation and electron-phonon interaction is thoroughly investigated within a range of values of the pulse duration (i.e. from 10fs to 2.3ps). The theoretical model elaborates firstly on possible transient changes of optical parameters during irradiation due to the presence of the non-equilibrium electrons and the modification of the electron distribution function in a material characterized by a variable electron density of states around the Fermi energy. The model correlates the role of nonthermal electrons, relaxation processes and induced stress-strain fields. Simulations are presented by choosing Nickel (Ni) as a test material to compute electron-phonon relaxation time due to its large electron-phonon coupling constant that expects to reveal more conclusively the influence of the non-equilibrium electrons. We demonstrate the consideration of the above factors leads to significant changes compared to the results the traditional Two Temperature Model (TTM) provides. We envisage that the parametric exploration could provide significant information related to induced surface morphological changes on the irradiated material.

PACS: 79.20.Ds, 62.20.D, 78.20.Bh

I. INTRODUCTION

Material processing with ultra-short pulsed lasers has received considerable attention over the past decades due to its important technological applications, in particular in industry and medicine [1-9]. Rapid energy delivery and reduction of the heat-affected areas are the most pronounced advantages of the technique compared to effects induced by longer pulses [10], which reflect the merit of the method as a potential tool for laser-assisted fabrication at micro- and nano-scales. These abundant applications require a thorough knowledge of the fundamentals of laser interaction with the target material for enhanced controllability of the resulting modification of the target relief. Physical mechanisms that lead to surface modification have been explored both theoretically and experimentally [11-23].

In principle, the laser beam characteristics (wavelength, pulse duration, fluence, number of pulses, angle of incidence and beam polarisation state) determine the onset of the surface modification as energy absorption, electro-dynamical effects and relaxation processes are critical to the material heating. Recently, it was demonstrated that irradiation of Nickel with ultrashort pulsed lasers leads to a decrease of the periodicity of the excited surface plasmons if cylindrical vector polarised beams are used instead of beams with linear polarisation [24]. It was demonstrated that the spatial distribution of the vector beam leads to a modulation of the deposited energy and its absorption, electron excitation, electron-electron and electron-phonon scattering processes. Furthermore, we noted that the electron and lattice temperature equilibrium is reached at different times in the two types of polarisation

while the rest of the parameters of the laser beam (i.e. pulse duration, fluence) do not vary. On the other hand, a theoretically calculated temporal shift in the electron-phonon relaxation was also reported in works that consider the contribution of nonthermal electrons in the ultrafast electron dynamics and relaxation processes. More specifically, experimental observations related to the nonequilibrium dynamics of electron systems in metals shows nonthermalised electron distribution leads to a faster electron-phonon relaxation [25, 26]. Hence, to discriminate nonthermal electron-generated electron-phonon relaxation, it is necessary to investigate thoroughly the dynamics of nonthermal electron gas in these conditions.

It is well-known that after irradiation, the initial electron population is highly nonthermal while the traditional Two Temperature Model (TTM) [27] assumes a rapidly (instantaneous) thermalisation of the electronic distribution. Therefore, TTM yields an overestimation of the electronic temperature which has been also confirmed by pump-probe experiments [28]. To overcome the limitations of the TTM, analysis based on the Boltzmann's transport equations [29] or revised versions of the TTM [28, 30-32] have been proposed. As expected, differences with predictions from the TTM were more evident for very short pulses compared with the electron thermalisation time. For the sake of simplicity, some previous approaches assumed that the electron density of states (DOS) is constant around the Fermi energy [30] which constitutes a sufficient approximation for noble metals (i.e. Au, Cu, Ag), however, for transient metals such as Nickel (Ni) or Titanium (Ti) it is a rather crude consideration which is expected to lead to inaccurate results (see Fig.1) [33]; hence, a more rigorous approach is required to determine the combined influence of the nonthermal electrons and density of states.

To proceed with the influence of electronic excitation on the morphological changes, one aspect that has yet to be explored is the correlation of the pulse width, energy deposition, optical properties changes during the pulse duration and structural changes. In principle, morphological surface changes at low excitation levels are strongly related to stress generation as well as whether lattice temperatures induce large stresses (i.e. that exceeds the yield stress) [34]. It is known that although nonthermal electron interactions with thermal electrons and the lattice yield remarkably smaller maximum electron temperature they induce smaller maximum lattice temperature variations due to the large lattice heat capacity [30]. Nevertheless, it is important to investigate whether a material with a large electron-phonon coupling constant and a complex DOS around the Fermi energy behaves differently and significant lattice temperature changes occur which, in turn, is also reflected on an enhanced mechanical response.

The elucidation of the aforementioned feature is of paramount importance not only to understand further the underlying physical mechanisms of laser-matter interactions and ultrafast electron dynamics but also to associate the resulting thermal effects with the surface response which can be used to process systematically the material. Therefore, there is a growing interest to reveal the physics of the underlying processes from both a fundamental and application point of view.

To this end, we present an extension of the TTM which comprises: (i) the energy balance between the thermal electron and the lattice baths enriched with the contribution of nonthermal electrons and the influence of the DOS around the Fermi energy, (ii) a component that corresponds to the temporal evolution of the optical parameters during the pulse duration, (iii) a thermomechanical component that describes the mechanical response of the material due to material heating. In order to highlight the significance of the nonthermal electrons for materials with large and temperature dependent electron-lattice coupling constant, G_{el} , Ni is used. For the sake of simplicity, the investigation has been focused on single shot while a similar approach could be pursued in case of repetitive irradiation.

In the following section, we present the theoretical framework used to describe the physical mechanism and the components of the revised TTM (rTTM). Section III explains the numerical algorithm and the adaptation of the model to Ni. A systematic analysis of the results and the role of the nonthermal electron contribution are presented in Section IV while the energy exchange between electrons and lattice for small and large excitations is also investigated. We determine the thermalisation time of the laser-excited electron gas as a function of the pulse duration. The resulting morphological changes are correlated with the pulse duration through the computation of strain fields and displacements. Concluding remarks follow in Section V.

II. THEORETICAL MODEL

A. Laser Beam Profile and Non-equilibrium Electrons

The laser pulse at time t' is described by an energy flux (in 3D-space characterised by the Cartesian coordinates x, y, z), $I(t', x, y, z)$ given by the following expressions

$$-\frac{\partial I(t', x, y, z)}{\partial z} = \alpha(t', x, y, z) I(t', x, y, z) = W(t', x, y, z) \quad (3)$$

$$I(t', x, y, z=0) = (1 - R(t', x, y, z=0)) \frac{2\sqrt{\log(2)}}{\sqrt{\pi}\tau_p} \times \exp\left(-4\log(2)\left(\frac{t'-3\tau_p}{\tau_p}\right)^2\right) \times \exp\left(-\frac{x^2+y^2}{(R_0)^2}\right) \quad (4)$$

where $W(t', x, y, z)$ corresponds to the absorbed laser power density, α is the absorption coefficient, τ_p is the pulse duration and R_0 stands for the irradiation spot radius. For the sake of simplicity, it is assumed that the ballistic length of electrons for Ni is small and therefore it is neglected [35]. Based on a previous work by Carpena [30], it is assumed that within an infinitesimal time $\Delta t'$ laser photons will interact with electrons lying in occupied states below Fermi energy ε_F causing their excitation to previously unoccupied states above ε_F . As result, an infinitesimal nonthermal change Δf to the (Fermi-Dirac) electronic distribution $f(\varepsilon)$ will be produced which has the form

$$\Delta f(\varepsilon, t', x, y, z) = \delta_0(t', x, y, z) (f(\varepsilon - h\nu) \times [1 - f(\varepsilon)] - f(\varepsilon) [1 - f(\varepsilon + h\nu)]) \quad (5)$$

where $f(\varepsilon) = \{1 + \exp[(\varepsilon - \mu_f)/(k_B T_e)]\}^{-1}$ is the Fermi-Dirac distribution for electrons with energies ε and temperature T_e , $h\nu$ is the laser photon energy ($\sim 1.55\text{eV}$ for laser beam wavelength $\lambda_L=800\text{nm}$), μ_f is the chemical potential that is equal to ε_F at $T_e=0\text{K}$ and k_B is the Boltzmann constant. We note that comparing the underlying physics with the proposed processes in the case of noble metals [30], some significant changes have to be performed to describe nonthermal electron distribution and their influence in excitation, thermalisation and electron-phonon relaxation processes for transient materials (i.e. Ni or Ti). More specifically, it is evident (Fig.1) that at fluences large enough to produce very energetic electrons, the variation of the Fermi-Dirac distribution cannot be described by a step-like function for energies in the range $[\varepsilon_F - h\nu, \varepsilon_F + h\nu]$ [30]. It is noted that results in Fig.1 are normalised to 1 (through the parameter δ_0) to underline the discrepancy; it is evident

that a different shape of Δf contains a substantially large tail that becomes even bigger with increasing T_e . According to Fig.1, the non-zero change of the Fermi-Dirac distribution

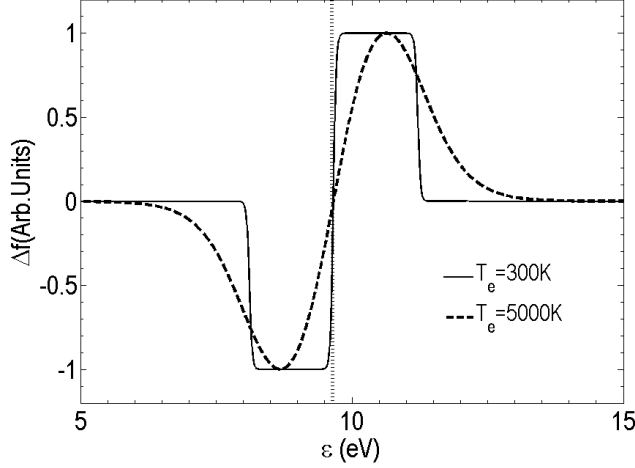


FIG. 1. Change of the Fermi-Dirac distribution function due to nonthermal electrons for $T_e=300\text{K}$ (solid line) and $T_e=5000\text{K}$ (dashed line). The dotted vertical line indicates the position of energy Fermi ε_F .

in a larger range of energies (characteristic for larger electron temperatures) requires consideration of the complete expression of the nonthermal electron distribution to estimate the correlation of the energy density associated with the nonthermal electrons and the absorbed laser power density. Simulations in the next sections illustrate differences in the resulting T_e , T_L and the thermomechanical response if a non-step-like variation for Δf is assumed. To estimate the size of Δf , according and then the relation of the nonthermal electron distribution, the DOS $N(\varepsilon)$ of the energies in that range and the absorbed energy is described by the following expression

$$\int_{\varepsilon_F - h\nu}^{\varepsilon_F + h\nu} \Delta f(\varepsilon, t', x, y, z) N(\varepsilon) \varepsilon d\varepsilon = W(t', x, y, z) dt' \quad (6)$$

which yields

$$\delta_0(t', x, y, z) = \frac{W(t', x, y, z) dt'}{\int_{\varepsilon_F - h\nu}^{\varepsilon_F + h\nu} (f(\varepsilon - h\nu)[1 - f(\varepsilon)] - f(\varepsilon)[1 - f(\varepsilon + h\nu)]) N(\varepsilon) \varepsilon d\varepsilon} \quad (7)$$

Furthermore, while it might be assumed that a constant DOS can be used for energies in the range $[\varepsilon_F - h\nu, \varepsilon_F + h\nu]$ for noble metals [33], it is rather a crude approximation for transient metals such as Ni (Fig.2). Due to the lack of a simple analytical expression for $N(\varepsilon)$ for energies in that range, the computation of Δf is derived through a numerical solution of Eq.(7). Fig.2 also indicates that the d -band

electrons can easily excited even at low electron temperatures.

On the other hand, the initial nonthermal electron distribution relaxes at a rate which is determined both from an electron-electron and electron-phonon interaction provided by the following expression [30]

$$\Delta f_{\text{NT}}(\varepsilon, t - t', x, y, z) = \exp\left(-\frac{t - t'}{\tau_{ee}} - \frac{t - t'}{\tau_{ep}}\right) \Delta f(\varepsilon, t', x, y, z) \quad (8)$$

where $\tau_{ee} = \frac{128}{\sqrt{3}\pi^2\omega_p} \left(\frac{\varepsilon_F}{\varepsilon - \varepsilon_F}\right)^2 \equiv \tau_0 \left(\frac{\varepsilon_F}{\varepsilon - \varepsilon_F}\right)^2$ and ω_p is the plasma frequency ($=15.92\text{eV}$ for Ni [36]) and $\varepsilon_F \approx 9.7\text{eV}$ for Ni [37]. By contrast, the electron-phonon collision is provided by the expression $\tau_{ep} = \frac{h\nu}{k_B\Theta_D} \tau_f$, where τ_f ($\approx 2.25\text{fs}$

for Ni [37]) stands for the time between two subsequent collisions with the lattice of nonthermal quasiparticles of energy $\varepsilon - \varepsilon_F \approx h\nu$ while Θ_D ($\Theta_D = 450\text{K}$, for Ni [38]) is the Debye temperature.

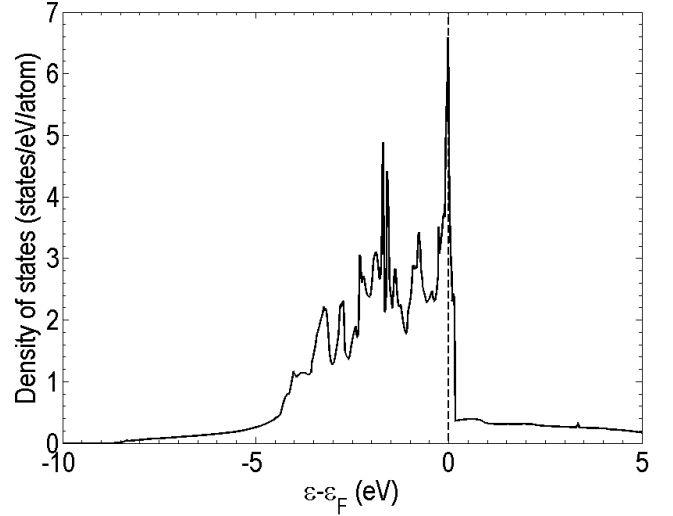


FIG. 2. The electron DOS of Ni (data calculated in Ref. [33]). The dashed vertical line indicates the position of the Fermi energy.

The rate of the energy density u that is transferred from the nonthermal electron distribution to both the thermal electrons and the lattice is described by the following expression

$$\begin{aligned}
\frac{\partial u(t, t')}{\partial t} &= \frac{\partial}{\partial t} \int_{\varepsilon_F - \hbar\nu}^{\varepsilon_F + \hbar\nu} \Delta f_{NT}(\varepsilon, t - t', x, y, z) N(\varepsilon) \varepsilon d\varepsilon \\
&= \int_{\varepsilon_F - \hbar\nu}^{\varepsilon_F + \hbar\nu} \frac{\partial}{\partial t} (\Delta f_{NT}(\varepsilon, t - t', x, y, z)) N(\varepsilon) \varepsilon d\varepsilon \\
&= - \int_{\varepsilon_F - \hbar\nu}^{\varepsilon_F + \hbar\nu} \left(\frac{1}{\tau_0} \left(\frac{\varepsilon - \varepsilon_F}{\varepsilon_F} \right)^2 + \frac{1}{\tau_{ep}} \right) \Delta f(\varepsilon, t', x, y, z) \times \\
&\quad \exp \left(- \frac{t - t'}{\tau_0} \left(\frac{\varepsilon - \varepsilon_F}{\varepsilon_F} \right)^2 - \frac{t - t'}{\tau_{ep}} \right) N(\varepsilon) \varepsilon d\varepsilon \\
&\equiv \frac{\partial u_{ee}(t, t')}{\partial t} + \frac{\partial u_{el}(t, t')}{\partial t}
\end{aligned} \tag{9}$$

where

$$\begin{aligned}
\frac{\partial u_{ee}(t, t')}{\partial t} &= - \frac{1}{\tau_0} \int_{\varepsilon_F - \hbar\nu}^{\varepsilon_F + \hbar\nu} \left(\frac{\varepsilon - \varepsilon_F}{\varepsilon_F} \right)^2 \Delta f(\varepsilon, t', x, y, z) \times \\
&\quad \exp \left(- \frac{t - t'}{\tau_0} \left(\frac{\varepsilon - \varepsilon_F}{\varepsilon_F} \right)^2 - \frac{t - t'}{\tau_{ep}} \right) N(\varepsilon) \varepsilon d\varepsilon
\end{aligned} \tag{10}$$

and

$$\begin{aligned}
\frac{\partial u_{el}(t, t')}{\partial t} &= - \left(\frac{1}{\tau_{ep}} \right) \int_{\varepsilon_F - \hbar\nu}^{\varepsilon_F + \hbar\nu} \Delta f(\varepsilon, t', x, y, z) \times \\
&\quad \exp \left(- \frac{t - t'}{\tau_0} \left(\frac{\varepsilon - \varepsilon_F}{\varepsilon_F} \right)^2 - \frac{t - t'}{\tau_{ep}} \right) N(\varepsilon) \varepsilon d\varepsilon
\end{aligned} \tag{11}$$

Finally, the total energy relaxation (i.e. at time t) that is transferred from the nonthermal electron distribution to both the thermal electrons and the lattice are derived by adding the infinitesimal contributions of excitation for time intervals dt' at all times $t' < t$. As a result, the following expressions are obtained by integrating over t' ,

$$\begin{aligned}
\frac{\partial U_{ee}(t)}{\partial t} &= \int_0^t \frac{\partial u_{ee}(t, t')}{\partial t} dt' \\
\frac{\partial U_{el}(t)}{\partial t} &= \int_0^t \frac{\partial u_{el}(t, t')}{\partial t} dt'
\end{aligned} \tag{12}$$

B. Dielectric constant

It is evident that the transient variation of the dielectric constant through the temperature dependence of the electron relaxation time will potentially produce a change of the optical properties of the material during irradiation. This variation cannot be ignored when the pulse duration is very small. A similar behaviour has been noted in noble metals (i.e. Au and Cu) where a static consideration of the optical properties led to an incorrect estimation of the energy deposition (i.e. its magnitude and spatial

distribution) which was reflected from an underestimation of the thermal response of the material and the damage threshold [39, 40]. Therefore, a more complete approach should be based on a rigorous approach of considering a dynamic change of the optical properties.

To take into account temperature dependence of the optical characteristics and incorporate both interband and intraband transitions, the dielectric constant of Ni is modelled by means of an extended Lorentz-Drude model with four Lorentzian terms based on the analysis of Rakic *et al.* [36]

$$\varepsilon(\omega_L) = 1 - \frac{f_0 \omega_p^2}{\omega_L^2 - i\Gamma_0 \omega_L} + \sum_{j=1}^{k=4} \frac{f_j \omega_p^2}{\omega_j^2 - \omega_L^2 + i\omega_L \Gamma_j} \tag{13}$$

where ω_L is the laser frequency ($= 2.3562 \times 10^{15}$ rad/s for 800nm that corresponds to photon energy equal to 1.55eV), and $\sqrt{f_0} \omega_p$ is the plasma frequency associated with oscillator strength f_0 and damping constant Γ_0 . The interband part of the dielectric constant (third term in Eq.13) assumes four oscillators with frequency ω_j , strength f_j , and lifetime $1/\Gamma_j$. Values for the aforementioned parameters are given in Ref.[36]. The damping constant Γ_0 is the reciprocal of the electron relaxation time, τ_e , which is given by $\tau_e = 1/(B_L T_L + A_e (T_e)^2)$, where T_e , T_L are the electron and lattice temperatures, respectively. Values of the coefficients A_e , B_L are 0.59×10^7 ($s^{-1} K^{-2}$) and 1.4×10^{11} ($s^{-1} K^{-1}$), respectively, which are obtained following a fitting approach based on results for Ni in Ref.[33, 34]. The dynamic character of the optical parameters (i.e. refractive index n , extinction coefficient k , absorption coefficient α , and reflectivity R) can be easily computed through the real and imaginary part of the dielectric constant ε_1 and ε_2 , respectively [41]

$$\begin{aligned}
\varepsilon(\omega_L, x, y, z, t) &= \varepsilon_1(x, y, z, t) + i\varepsilon_2(x, y, z, t) \\
n &= \sqrt{\frac{\varepsilon_1(x, y, z, t) + \sqrt{(\varepsilon_1(x, y, z, t))^2 + (\varepsilon_2(x, y, z, t))^2}}{2}} \\
k &= \sqrt{\frac{-\varepsilon_1(x, y, z, t) + \sqrt{(\varepsilon_1(x, y, z, t))^2 + (\varepsilon_2(x, y, z, t))^2}}{2}} \\
\alpha(x, y, z, t) &= \frac{2\omega_L k}{c} \\
R(x, y, z = 0, t) &= \frac{(1-n)^2 + k^2}{(1+n)^2 + k^2}
\end{aligned} \tag{14}$$

C. Elasticity Equations

The mechanical response of the material is described by the differential equations of dynamic elasticity which correlate the stress and strain generation and the induced displacement as a result of the thermal expansion and the

lattice temperature variation

$$\begin{aligned} \rho_L \frac{\partial^2 V_i}{\partial t^2} &= \sum_{j=1}^3 \frac{\partial \sigma_{ij}}{\partial x^j} \\ \sigma_{ij} &= 2\mu \varepsilon_{ij} + \lambda \sum_{k=1}^3 \varepsilon_{kk} \delta_{ij} - \delta_{ij} (3\lambda + 2\mu) \alpha' (T_L - T_0) \\ \varepsilon_{ij} &= 1/2 \left(\frac{\partial V_i}{\partial x^j} + \frac{\partial V_j}{\partial x^i} \right) \end{aligned} \quad (15)$$

where V_i correspond to the displacements along the x ($i=1$), y ($i=2$), z ($i=3$) direction, while σ_{ij} and ε_{ij} stand for the stresses and strains, respectively [42]. On the other hand, the Lamé's coefficients λ and μ (for Ni, $\lambda=1.25 \times 10^7$ and $\mu=7.63 \times 10^7$), respectively, α' stands for the thermal expansion of Ni and ρ_L is the density of the material. The Lamé's coefficients λ and μ are related to the Poisson's ration (ν) and Young's modulus (E) through the relations $\nu = \lambda / (2(\lambda + \mu))$ and $E = \mu(2\mu + 3\lambda) / (\lambda + \mu)$.

D. Generalised Energy Balance Equations

To describe the influence of the ultrafast electron dynamics the relaxation procedure, and the thermomechanical response of the material, a revised version of the TTM is used that includes the early and transient interaction of the non-thermal electron distribution with the electron and lattice baths [30, 31]. Hence, the following set of equations is employed to investigate the spatio-temporal distribution of the produced thermalized electron (T_e) and lattice (T_L) temperatures of the assembly

$$\begin{aligned} C_e \frac{\partial T_e}{\partial t} &= \vec{\nabla} \cdot (k_e \vec{\nabla} T_e) - G_{eL} (T_e - T_L) + \frac{\partial U_{ee}}{\partial t} \\ C_L \frac{\partial T_L}{\partial t} &= G_{eL} (T_e - T_L) + \frac{\partial U_{eL}}{\partial t} - (3\lambda + 2\mu) \alpha' T_L \sum_{j=1}^3 \hat{\varepsilon}_{jj} \end{aligned} \quad (16)$$

where the subscripts e and L are associated with electrons and lattice, respectively, k_e ($=k_{e0} B T_e / (A(T_e)^2 + B T_L)$) is the thermal conductivity of the electrons, C_e and C_L are the heat capacity of electrons and lattice, respectively, and G_{eL} is the electron-phonon coupling factor.

III. NUMERICAL SOLUTION

Due to the inherent complexity of Eqs.(1-16), an analytical solution is not feasible and therefore, a numerical approach is pursued. Numerical simulations have been performed using the finite difference method while the discretization of time and space has been chosen to satisfy the Neumann stability criterion. Furthermore, it is assumed that on the boundaries, von Neumann boundary conditions are satisfied and heat losses at the front and back surfaces of the

material are negligible. The initial conditions are $T_e(t=0)=T_L(t=0)=300\text{K}$, while stresses, strains, and displacements are set to zero at $t=0$. Furthermore, the vertical stress σ_{zz} of the upper surface is taken to be zero at all times (i.e. stress free). The parameters for Ni used in the simulation are summarised in Table I.

TABLE I: Parameters for Ni

| Parameter | Value |
|---|--------------|
| C_e [$10^5 \text{ J/m}^3\text{K}$] | Fitting [33] |
| C_L [$\text{J Kgr}^{-1} \text{ K}^{-1}$] | Fitting [43] |
| G_{eL} [$10^{17} \text{ Wm}^{-3}\text{K}^{-1}$] | Fitting [33] |
| A [$10^7 \text{ s}^{-1} \text{ K}^{-2}$] | 0.59 |
| B [$10^{11} \text{ s}^{-1} \text{ K}^{-1}$] | 1.4 |
| k_{e0} [$\text{Jm}^{-1}\text{s}^{-1}\text{K}^{-1}$] | 90 |
| T_{melt} [K] | 1728 |
| T_0 [K] | 300 |
| α' [10^{-6}K^{-1}] | 13.4 |
| E [GPa] | 200 |
| ν | 0.31 |
| ρ_L [Kgr/m^3] | 8908 |
| ε_F [eV] | 9.7 |

The values of the laser beam used in the simulation are:

The (peak) fluence is $E_p \left(\equiv \sqrt{\pi} \tau_p I_0 / (2\sqrt{\ln 2}) \right) = 40 \text{ mJ/cm}^2$,

where I_0 stands for the peak value of the intensity, spot radius R_0 (where the intensity falls to $1/e^2$) is equal to $15 \mu\text{m}$, and pulse duration values lie in the range [10fs, 2.5ps]. The wavelength of the beam is $\lambda_L=800\text{nm}$. We note that, for the sake of simplicity, the laser beam conditions used in the simulations in this work are chosen so that: (i) they emphasise the role of the nonthermal electrons and (ii) they are not sufficient to lead to material melting or lead to plastic deformation. Hence, only elastic deformation of portion of the material is assumed. In a previous work, melting and disintegration of Nickel films were explored after irradiation with ultrashort pulses by using a combined atomistic-continuum modelling [44]. A common approach followed to solve problems that involve elastic displacements [42] or hydrodynamics [11] is the employment of a staggered grid finite difference method which is found to be effective in suppressing numerical oscillations. Unlike the conventional finite difference method, temperatures (T_e and T_L) and normal stresses σ_{ii} are computed at the centre of each element while time derivatives of the displacements and first-order spatial derivative terms are evaluated at locations midway between consecutive grid points. Furthermore, shear stresses σ_{ij} are evaluated at the grid points. Numerical integration is allowed to move to the next time step provided that all variables at every element satisfy a predefined convergence tolerance of $\pm 0.1\%$.

IV. RESULTS-DISCUSSION

The contribution of the nonthermal electron and its interactions with the thermal electrons needs to be evaluated and be tested whether it is reflected on the optical property changes of the material and thereby the energy deposition and absorption. As a result, it is necessary to explore possible temporal changes of the reflectivity and absorption coefficient during the pulse duration before they are integrated into the rate equations (Eqs.16). In principle, a thorough investigation of the optical property changes is required as any change is expected to influence, firstly, excitation and relaxation processes, and secondly, the thermal and mechanical response of the material. However, theoretical results for three different pulse duration values ($\tau_p=10\text{fs}$, 50fs and 170fs) indicate that the transient optical property changes are very small during the period in which the laser is on (Fig.3) and therefore both reflectivity and absorption coefficient variations are not expected to influence substantially the thermomechanical response of the system. Similarly small changes are predicted for other values of the pulse duration. Nevertheless, to provide a more rigorous exploration of the fundamental processes, the calculated transient behaviour is incorporated into Eq.16.

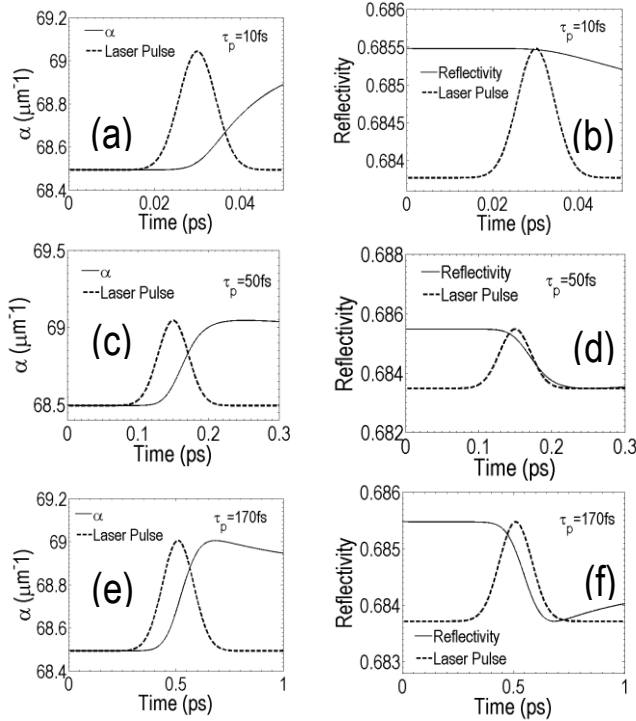


FIG. 3. (Color online) Temporal dependence of absorption coefficient and reflectivity for two different values of pulse duration, ($\tau_p=10\text{fs}$, 50fs and 170fs). ($E_p=40\text{mJ/cm}^2$, 800nm laser wavelength, $R_0=15\mu\text{m}$).

Next, to determine the role of the nonthermal electrons in the heat exchange and relaxation process, it is important to provide a computed estimate of the energy density per unit time stored in the nonthermal electronic distribution. Fig.4 illustrates the power density which in the traditional TTM is stored in the electron system while the net result of the contribution of $\partial U_{ee}/\partial t$ and $\partial U_{eL}/\partial t$ indicates the large amount of overestimation of the internal energy of the thermal electrons. It is evident from the temporal profile of the lattice heat source that electron-electron scattering dominates in the initial stages due to the small electron-phonon coupling. The significant nonthermal electron-lattice interaction in transition metals is attributed to the large electron-phonon coupling. A comparison of the maximum surface electron and lattice temperatures as a function of time (for four different pulse durations, $t_p=10\text{fs}$, 50fs , 170fs , and 1.5ps) simulated with the traditional TTM and rTTM is presented in Fig. 5. It is evident from viewing and comparing the two models that the electron temperature peak is reached with a short delay with respect to the value attained if the TTM model is employed. This consequence is ascribed to the erroneously assumption of an instantaneous creation of thermal electrons and heating process of the electron and lattice baths predicted from the TTM model; in practice, there is a finite time required for the creation of the nonthermal electrons which leads to a delayed heating of both the thermal electrons and lattice (Fig.6). This delay is more pronounced for small pulse durations rather than longer excitation periods ($\tau_p=1.5\text{ps}$).

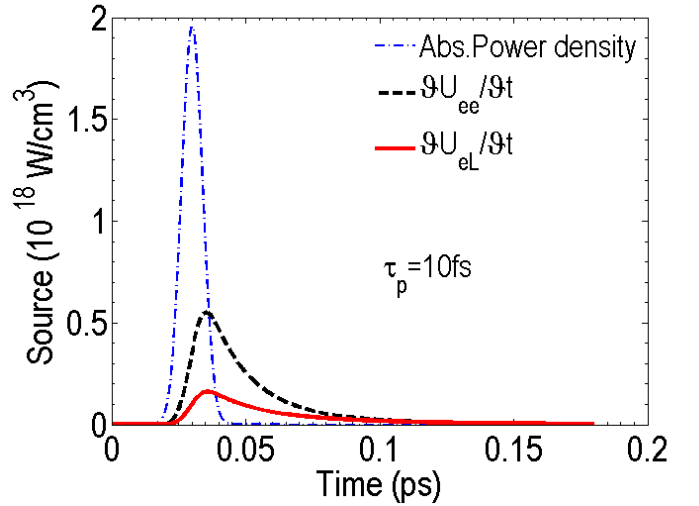


FIG. 4. (Color online) Time evolution of: (i) the laser source power density (*dashed-dotted* line), (ii) $\partial U_{ee}/\partial t$ (*dashed* line) and (iii) $\partial U_{eL}/\partial t$ (*solid* line) at maximum intensity for Ni irradiated with 10fs laser beams ($E_p=40\text{mJ/cm}^2$, 800nm laser wavelength, $R_0=15\mu\text{m}$).

This is also illustrated in Fig.4 where it is evident that maximum power density transferred to the thermal

electrons and lattice systems (*dashed* and *solid* lines, respectively) is shifted compared to whether it is assumed that instantaneous electron thermalisation occurs (*dashed dotted* line). The employment of the revised model indicates that the incorporation of the contribution of the nonthermal electrons lowers the electron temperature. The decrease of the electron temperature is a physical outcome of the electron energy loss due mainly to the scattering of the nonthermal electrons from the electronic bath. By contrast, a comparison of the T_e and T_L evolution curves demonstrates that despite the delayed heating of the electron and lattice systems, respectively, electron-phonon relaxation is expected earlier if the rTTM is used (Fig.5). This is a reasonable outcome because the revised model predicts smaller maximum electron temperatures. As a result, for Nickel, the electron-phonon coupling increases with decreasing T_e [33] which leads to faster relaxation process. By contrast, this discrepancy is expected to decrease for larger pulse durations as the significant role of the nonthermal electrons is weaker (Fig.5d).

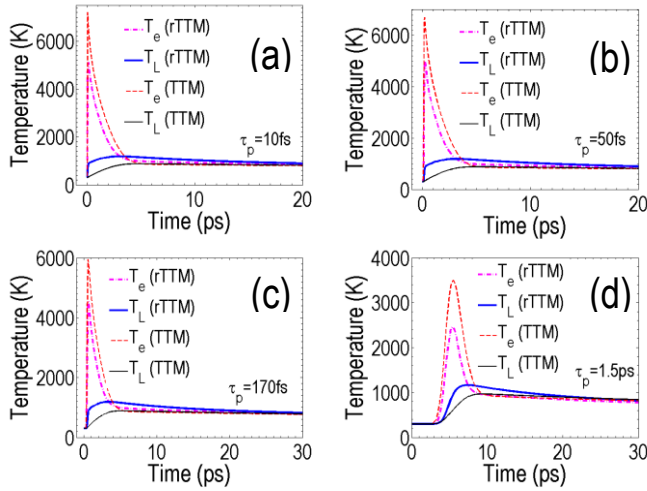


FIG. 5. (Color online) Electron and lattice evolution for $\tau_p=10$ fs (a), 50fs (b), 170fs (c), and 1.5ps (d) derived from rTTM and TTM. ($E_p=40$ mJ/cm², 800nm laser wavelength, $R_0=15\mu$ m).

By contrast, the electron-phonon interaction accounts for the increase of the lattice temperature, which is further enhanced by the term that describes the interaction of the nonthermal electrons with the lattice (i.e. $\partial U_{el}/\partial t$).

Thermal response of the system has been quantified for various pulse duration values in the range [10fs, 2.5ps] and the predicted values of the maximum electron and lattice temperatures are illustrated in Fig.7. The decrease of the maximum electron temperature with increasing pulse duration is illustrated in the graph while a small increase of the lattice temperature is produced. The computed value for the lattice temperature is $T_L^{rTTM} \sim 1191$ K and $T_L^{TTM} \sim 1000$ K. The 19% increase with respect to the value predicted by the

classical TTM is very significant as it demonstrates that the damage threshold (i.e. laser fluence that causes surface modification on the material) decreases if the nonthermal electron interaction with lattice is assumed. It is noted that the fluence value used in this simulations was properly chosen so that the produced lattice temperatures do not lead to either thermoplastic effects or phase transition. Therefore, the discrepancy of the values predicted by the two approaches is expected to increase if higher fluences are used which suggests that damage threshold decreases even further if the rTTM is employed.

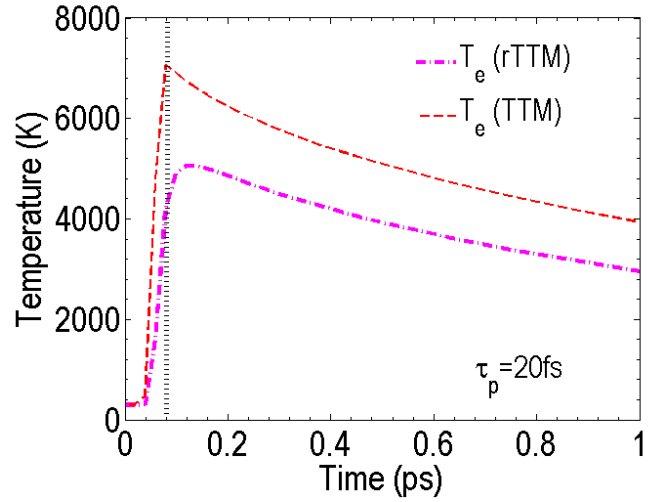


FIG. 6. (Color online) Maximum electron temperature evolution computed using rTTM (*dashed dotted* line) or TTM (*dashed* line) for $\tau_p=20$ fs. Vertical *dotted* line indicates the heating delay of the electron system. ($E_p=40$ mJ/cm², 800nm laser wavelength, $R_0=15\mu$ m).

Variation of the lattice temperature induced by the absorption of the ultrashort optical pulse leads to mechanical effects due to the generation of thermal stresses. Thermal stress produces strain generation and propagation. The spatio-temporal strain/stress pulse shape is determined by the solution of Eqs.15-16. To emphasise on the differences of the magnitude and spatial distribution of the strains and stresses predicted by the rTTM and TTM, the components of these fields along the direction of energy propagation (z -axis) are calculated and illustrated in Fig.8 and Fig.9, respectively. The strain ϵ_{zz} is always positive at $z=0$ due to the fact the stress free boundary condition does not imply any stretching perpendicular to the free surface. Furthermore, the solution of the second order (with respect to time) differential equation for the displacements (first equation of Eq.15) yields a two term propagating part, one showing a positive strain and a second with symmetric negative strain (result of the reflection on the surface). The two terms exhibit an exponential decay with length equal to $1/a$. The exponential decay is reflected also on the stress

fields which offer a more accurate calculation of the exponential decay length (Fig.9). Similar results for the strain pulse propagation have been presented in previous works for picosecond light pulses [45, 46]. Furthermore, reflectivity changes due to strain generation after ultrashort-pulsed laser irradiation of thin films on silicon surfaces have been also recently investigated [34, 47]. Comparing the strain values at $z=0$ with the results predicted in previous works ([45, 46]), the nonconstant $\varepsilon_{zz}(z=0,t)$ at all times is attributed to the fact that in the current simulations, lattice temperature rise after irradiation neither occurs instantaneously nor remains constant.

It is evident by estimating the spatial position of the lowest strain or stress values at different times (Fig.8,9) that the strain and stress pulses propagate at a speed equal to, approximately, 5578m/sec which corresponds to the longitudinal sound velocity in Ni ($=\sqrt{(2\mu+\lambda)/\rho_L}$ [46]). The pulses are illustrated at four different timepoints, $t=8$ ps, 15ps, 20ps, and 30ps, after the arrival of the laser pulse on the surface of the material.

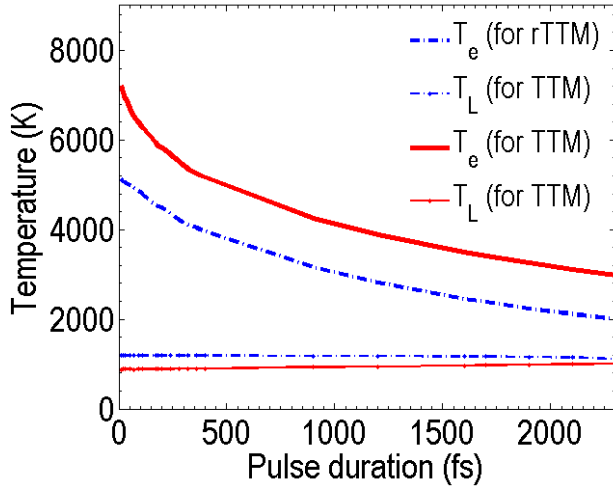


FIG. 7. (Color online) Maximum electron and lattice temperatures as a function of the laser pulse duration ($E_p = 40\text{mJ/cm}^2$, 800nm laser wavelength, $R_0=15\mu\text{m}$).

The comparison of the ε_{zz} and σ_{zz} pulses using rTTM and TTM demonstrates firstly the temporal shift of the waves that result from the delay of the lattice heating predicted by the revised model. Furthermore, the shapes of the strain and stress pulses derived from the two models do not appear to be significantly different at large timepoints. By contrast, there exists a larger than 20% increase in both the strain and stress size in a region *near* the surface at small times after laser irradiation (see Fig.9 and Supplementary Material [48]). A similarly substantially large deviation is also evident at bigger depths and more specifically, in the range $[5t/\alpha\sqrt{(2\mu+\lambda)/\rho_L}/120, 5t/\alpha\sqrt{(2\mu+\lambda)/\rho_L}/80]$. The

deviations are attributed to the enhanced lattice temperature values produced by the nonthermal electron interaction with lattice which is very pronounced at small timepoints while relaxation to values comparable to the ones predicted by the TTM is expected at bigger times (Fig.5).

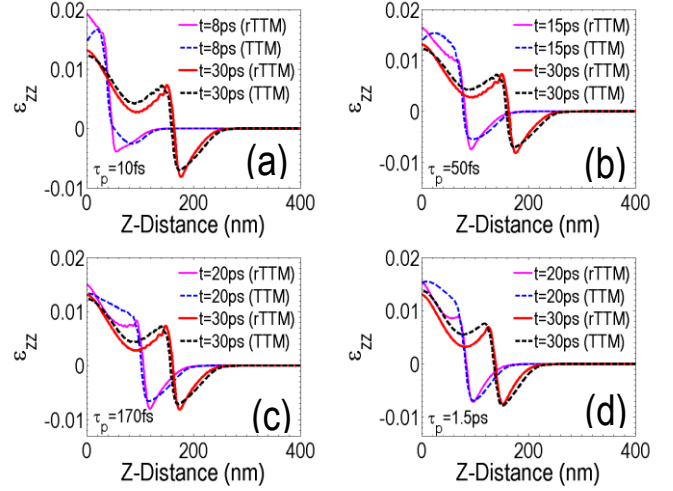


FIG. 8. (Color online) Spatial dependence of strain along z -direction (at $x=0$) at $t=8$ ps, 15ps, 20ps, and 30ps for $\tau_p=10$ fs, 50fs, 170fs, and 1.5ps derived from rTTM and TTM. ($E_p = 40\text{mJ/cm}^2$, 800nm laser wavelength, $R_0=15\mu\text{m}$).

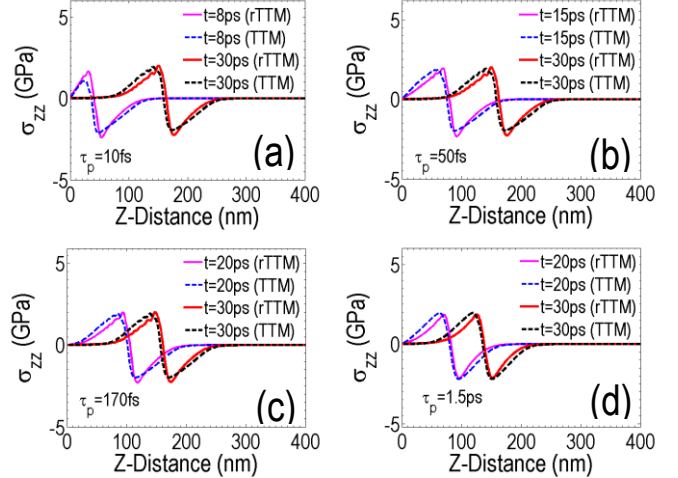


FIG. 9. (Color online) Spatial dependence of stress along z -direction (at $x=0$) at $t=8$ ps, 15ps, 20ps, and 30ps for $\tau_p=10$ fs, 50fs, 170fs, and 1.5ps derived from rTTM and TTM. ($E_p = 40\text{mJ/cm}^2$, 800nm laser wavelength, $R_0=15\mu\text{m}$).

Certainly, an experimental validation of the proposed mechanism is required to test the adequacy of the theoretical model. Nevertheless, the aforementioned results related to the thermomechanical response of the material confirm the primary importance of the proposed underlying physical mechanism of laser matter interaction and associated processes. Although, single shot laser irradiation

at low fluence does not appear to influence the strain/stress fields shape (at larger times) if the role of the nonthermal electrons is taken into account, the picture, however, is expected to alter drastically in different laser conditions. For example, in multiple shot experiments of small temporal delays between the subsequent pulses (i.e. train-pulse technology), the approximately 20% variation of the strain wave amplitude or the substantially smaller electron temperature produced due to excitation could influence (through accumulation effects) surface micromachining techniques and applications. Furthermore, the significant deviation of the magnitude of the strain fields at small timepoints (i.e. ~ 8 ps) could also influence mechanical properties of bilayered materials (for example, thin films on silicon surfaces [34, 47]) where strong acoustic waves are expected to be reflected on the interface and interfere strongly with the propagating strain leading to a more complex total strain.

Another significant aspect is related to the impact of the discrepancy between the predicted maximum lattice temperatures derived from the two models. This prospect is expected to have a very important impact on material properties and industrial applicability in terms of capability to modulate laser parameters as it will provide a more accurate and precise range of fluences to avoid surface damage.

V. CONCLUSIONS

A detailed theoretical framework was presented that describes both the ultrafast dynamics of electrons and the induced strains and stresses in metals with strong electron-phonon coupling and complex DOS after irradiation with ultrashort pulsed lasers. The revised TTM (i.e. rTTM) incorporates the interaction of the nonthermal electrons with both the thermal electrons and the lattice while an additional component is included to describe the thermomechanical effects. A parametric analysis was performed for a range of pulse duration values that emphasizes the limitations of the classical TTM to describe efficiently electron dynamics and relaxation processes. Elucidation of the underlying mechanism that assumes the role of the nonthermal electron does not only allow control and alteration of the optoelectronic properties of the material but also enhances our understanding of the mechanical response of the irradiated system. It is demonstrated that the employment of the revised TTM yields remarkably large values for the induced strains especially at small timepoints after irradiation which is expected to be of paramount importance depending on the laser processing techniques (i.e. laser-pulse train processing). Furthermore, the elucidation of the fundamental physical mechanisms is expected to provide a more precise determination of the damage threshold of the material.

ACKNOWLEDGEMENTS

G.D.T acknowledges financial support from *LiNaBioFluid* (funded by EU's H2020 framework programme for research and innovation under Grant agreement No 665337) and *Nanoscience Foundries and Fine Analysis (NFFA)–Europe* H2020-INFRAIA-2014-2015 (under Grant agreement No 654360).

*Corresponding author: tsibidis@iesl.forth.gr

- [1] A. Y. Vorobyev and C. Guo, *Laser & Photonics Reviews* **7**, 385 (2012).
- [2] V. Zorba, L. Persano, D. Pisignano, A. Athanassiou, E. Stratakis, R. Cingolani, P. Tzanetakis, and C. Fotakis, *Nanotechnology* **17**, 3234 (2006).
- [3] V. Zorba, E. Stratakis, M. Barberoglou, E. Spanakis, P. Tzanetakis, S. H. Anastasiadis, and C. Fotakis, *Advanced Materials* **20**, 4049 (2008).
- [4] D. Bäuerle, *Laser processing and chemistry* (Springer, Berlin ; New York, 2000), 3rd rev. enlarged edn.
- [5] J.-C. Diels and W. Rudolph, *Ultrashort laser pulse phenomena : fundamentals, techniques, and applications on a femtosecond time scale* (Elsevier / Academic Press, Amsterdam ; Boston, 2006), 2nd edn., Optics and photonics.
- [6] E. L. Papadopoulou, A. Samara, M. Barberoglou, A. Manousaki, S. N. Pagakis, E. Anastasiadou, C. Fotakis, and E. Stratakis, *Tissue Eng Part C-Me* **16**, 497 (2010).
- [7] Z. B. Wang, M. H. Hong, Y. F. Lu, D. J. Wu, B. Lan, and T. C. Chong, *Journal of Applied Physics* **93**, 6375 (2003).
- [8] C. A. Zuhlke, T. P. Anderson, and D. R. Alexander, *Optics Express* **21**, 8460 (2013).
- [9] M. Konstantaki, P. Childs, M. Sozzi, and S. Pissadakis, *Laser & Photonics Reviews* **7**, 439 (2013).
- [10] B. N. Chichkov, C. Momma, S. Nolte, F. vonAlvensleben, and A. Tunnermann, *Applied Physics a-Materials Science & Processing* **63**, 109 (1996).
- [11] G. D. Tsibidis, M. Barberoglou, P. A. Loukakos, E. Stratakis, and C. Fotakis, *Physical Review B* **86**, 115316 (2012).
- [12] G. D. Tsibidis, C. Fotakis, and E. Stratakis, *Physical Review B* **92**, 041405(R) (2015).
- [13] G. D. Tsibidis, E. Stratakis, P. A. Loukakos, and C. Fotakis, *Applied Physics A* **114**, 57 (2014).
- [14] T. J. Y. Derrien, T. E. Itina, R. Torres, T. Sarnet, and M. Sentis, *Journal of Applied Physics* **114**, 083104 (2013).
- [15] J. Z. P. Skolski, G. R. B. E. Romer, J. V. Obona, V. Ocelik, A. J. H. in 't Veld, and J. T. M. De Hosson, *Physical Review B* **85**, 075320 (2012).
- [16] J. Bonse, J. Krüger, S. Höhm, and A. Rosenfeld, *Journal of Laser Applications* **24**, 042006 (2012).
- [17] F. Garrelie, J. P. Colombier, F. Pigeon, S. Tonchev, N. Faure, M. Bounhalli, S. Reynaud, and O. Parriaux, *Optics Express* **19**, 9035 (2011).
- [18] J. Wang and C. Guo, *Applied Physics Letters* **87**, 251914 (2005).
- [19] M. Huang, F. L. Zhao, Y. Cheng, N. S. Xu, and Z. Z. Xu, *Acs Nano* **3**, 4062 (2009).
- [20] J. Bonse and J. Kruger, *Journal of Applied Physics* **108**, 034903 (2010).
- [21] G. D. Tsibidis, E. Skoulas, A. Papadopoulos, and E. Stratakis, *Physical Review B* **94**, 081305(R) (2016).
- [22] S. M. Petrovic, B. Gakovic, D. Perusko, E. Stratakis, I. Bogdanovic-Radovic, M. Cekada, C. Fotakis, and B. Jelenkovic, *Journal of Applied Physics* **114**, 233108 (2013).
- [23] Y. Shimotsuma, P. G. Kazansky, J. R. Qiu, and K. Hirao, *Physical Review Letters* **91**, 247405 (2003).
- [24] G. D. Tsibidis, E. Skoulas, and E. Stratakis, *Optics Letters* **40**, 5172 (2015).
- [25] R. H. M. Groeneveld, R. Sprik, and A. Lagendijk, *Physical Review B* **45**, 5079 (1992).
- [26] N. Del Fatti, C. Voisin, M. Achermann, S. Tzortzakis, D. Christofilos, and F. Vallée, *Physical Review B* **61**, 16956 (2000).
- [27] S. I. Anisimov, Kapeliov.BI, and T. L. Perelman, *Zhurnal Eksperimentalnoi Teor. Fiz.* **66**, 776 (1974 [Sov. Phys. Tech. Phys. **11**, 945 (1967)]).
- [28] M. Lisowski, P. A. Loukakos, U. Bovensiepen, J. Stahler, C. Gahl, and M. Wolf, *Applied Physics a-Materials Science & Processing* **78**, 165 (2004).
- [29] B. Rethfeld, A. Kaiser, M. Vicanek, and G. Simon, *Physical Review B* **65**, 214303 (2002).
- [30] E. Carpene, *Physical Review B* **74**, 024301 (2006).
- [31] G. D. Tsibidis, *Applied Physics Letters* **104**, 051603 (2014).
- [32] C. K. Sun, F. Vallee, L. H. Acioli, E. P. Ippen, and J. G. Fujimoto, *Physical Review B* **50**, 15337 (1994).
- [33] Z. Lin, L. V. Zhigilei, and V. Celli, *Physical Review B* **77**, 075133 (2008).
- [34] E. Tzianaki, M. Bakarezos, G. D. Tsibidis, Y. Orphanos, P. A. Loukakos, C. Kosmidis, P. Patsalas, M. Tatarakis, and N. A. Papadogiannis, *Optics Express* **23**, 17191 (2015).

- [35] J. Hohlfeld, S. S. Wellershoff, J. Gudde, U. Conrad, V. Jahnke, and E. Matthias, *Chemical Physics* **251**, 237 (2000).
- [36] A. D. Rakic, A. B. Djurić, J. M. Elazar, and M. L. Majewski, *Applied Optics* **37**, 5271 (1998).
- [37] S. Halas and T. Durakiewicz, *Journal of Physics-Condensed Matter* **10**, 10815 (1998).
- [38] C. Kittel, *Introduction to solid state physics* (Wiley, Hoboken, NJ, 2005), 8th edn.
- [39] Y. P. Ren, J. K. Chen, and Y. W. Zhang, *Journal of Applied Physics* **110**, 113102 (2011).
- [40] Y. P. Ren, J. K. Chen, Y. W. Zhang, and J. Huang, *Applied Physics Letters* **98**, 191105 (2011).
- [41] M. Born and E. Wolf, *Principles of optics : electromagnetic theory of propagation, interference and diffraction of light* (Cambridge University Press, Cambridge ; New York, 1999), 7th expanded edn.
- [42] G. D. Tsibidis, E. Stratakis, and K. E. Aifantis, *Journal of Applied Physics* **111**, 053502 (2012).
- [43] M. W. Chase, J. L. Curnutt, J. R. Downey, R. A. McDonald, A. N. Syverud, and E. A. Valenzuela, *J Phys Chem Ref Data* **11**, 695 (1982).
- [44] D. S. Ivanov and L. V. Zhigilei, *Physical Review B* **68**, 064114 (2003).
- [45] C. Thomsen, H. T. Grahn, H. J. Maris, and J. Tauc, *Physical Review B* **34**, 4129 (1986).
- [46] O. Matsuda, M. C. Larciprete, R. Li Voti, and O. B. Wright, *Ultrasonics* **56**, 3 (2015).
- [47] E. Tzianaki, M. Bakarezos, G. D. Tsibidis, S. Petrakis, P. A. Loukakos, C. Kosmidis, M. Tatarakis, and N. A. Papadogiannis, *Applied Physics Letters* **108**, 254102 (2016).
- [48] See Supplementary Material at [URL] that shows videos that describe the spatio-temporal distribution of ε_{zz} and σ_{zz} for $\tau_p=10, 50, 170$ fs and 1.5ps.